communications earth & environment

Article

https://doi.org/10.1038/s43247-024-01383-x

# Last Interglacial subsurface warming on the Antarctic shelf triggered by reduced deep-ocean convection

Check for updates

Nicholas King-Hei Yeung [1,2] ✉, Laurie Menviel [1,3], Katrin J. Meissner [1,2], Dipayan Choudhury[1,2], Tilo Ziehn [4] & Matthew A. Chamberlain[5]

The Antarctic ice-sheet could have contributed 3 to 5 m sea-level equivalent to the Last Interglacial sea-level highstand. Such an Antarctic ice-mass loss compared to pre-industrial requires a subsurface warming on the Antarctic shelf of ~ 3 °C according to ice-sheet modelling studies. Here we show that a substantial subsurface warming is simulated south of 60 °S in an equilibrium experiment of the Last Interglacial. It averages +1.2 °C at ~ 500 m depth from 70 °W to 160 °E, and it reaches +2.4 °C near the Lazarev Sea. Weaker deep-ocean convection due to reduced sea-ice formation is the primary driver of this warming. The associated changes in meridional density gradients and surface winds lead to a weakened Antarctic Circumpolar Current and strengthened Antarctic Slope Current, which further impact subsurface temperatures. A subsurface warming on the Antarctic shelf that could trigger ice-mass loss from the Antarctic ice-sheet can thus be obtained during warm periods from reduced sea-ice formation.

The Last Interglacial (LIG, ~ 129 to 116 thousand years before present, hereafter ka) was probably the warmest interglacial period of the last 800 ka[1]. While the concentration of atmospheric $CO_2$ was 10 ppm lower at the peak of the LIG ( ~ 127 ka; 275 ppm) than during the pre-industrial period (PI, 1850 CE)[2], the Earth's orbital parameters were such that the mean insolation north of 60 °N was 47 W $m^{-2}$ higher between May and July, and 45 W $m^{-2}$ lower between August and September. At high southern latitudes (south of 60 °S), it was 46 W $m^{-2}$ higher between August and October, but 36 W $m^{-2}$ lower between December and February (Fig. S1).

The global mean sea-level (GMSL) at the LIG was likely ~ 3-6 m higher than during PI, although estimates range from 1.2 m to 9.4 m[3–5]. A compilation of sea-level geological records from 42 localities suggested that the LIG peak GMSL was 6.6 to 9.4 m above present-day[5]. A subsequent reconstruction based on coral U-Th ages agreed with this figure, estimating a range between 5.5 and 9 m GMSL above present[3]. However, a recent study revised LIG sea-level data across the Bahamas with a suite of glacial isostatic adjustment models to suggest that the LIG GMSL peak was at least 1.2 m but unlikely more than 5.3 m above PI[4]. While there are still large uncertainties associated with the exact timing of the peak GMSL and potential centennial to millennial-scale sea-level variability during the LIG[6], most studies suggest a highstand between ~ 130 and 125 ka[5,7].

It is estimated that the mean ocean temperature peaked at 129 ka, leading to a maximum of 0.7 m thermosteric sea-level rise[8]. While paleo-proxy records and modelling studies suggest a possible Greenland ice-sheet (GrIS) contribution of 0.6 to 5.1 m sea-level equivalent (s.l.e), with a mean contribution of 2 m s.l.e., most studies suggest that the GrIS ice-mass loss occurred after 125 ka[7,9–12]. This implies that the Antarctic ice-sheet (AIS) was the major contributor to the early LIG highstand, with possible estimates between 3 and 7.4 m s.l.e[5,7,10]. A recent study agrees with this range, suggesting the AIS contribution to be of maximum 5.7 m (with 3.6 to 8.7 m central 68% probability)[13]. An early LIG ice-mass loss from the West AIS is consistent with a Southern Ocean authigenic uranium record, indicating enhanced stratification due to meltwater input[14]. A retreat of the West AIS in the early LIG has also been suggested by a blue ice record[15], while sedimentological and geochemical records suggest a retreat of the Wilkes Subglacial Basin in East Antarctica during the LIG[16].

The processes leading to a substantial ice-mass loss from Antarctica at the LIG are, however, poorly constrained. In order to simulate an Antarctic ice volume lower than today, Antarctic ice-sheet models have to be forced by a subsurface warming on the Antarctic shelf on the order of 3 °C[17,18]. Whether such a large subsurface warming on the continental shelf at the LIG is possible remains to be demonstrated. To address this

[1]Climate Change Research Centre, University of New South Wales, Sydney, NSW, Australia. [2]ARC Centre of Excellence for Climate Extremes, University of New South Wales, Sydney, NSW, Australia. [3]The Australian Centre for Excellence in Antarctic Science, University of New South Wales, Sydney, NSW, Australia. [4]Oceans and Atmosphere, CSIRO, Aspendale, VIC, Australia. [5]Oceans and Atmosphere, CSIRO, Hobart, TAS, Australia. ✉e-mail: nicholas.yeung@unsw.edu.au

question, here we analyse the Southern Ocean subsurface temperature response to LIG boundary conditions, as simulated in the Coupled Model Intercomparison Project Phase 6 (CMIP6) – Paleoclimate Modelling Intercomparison Project 4 (PMIP4) *lig127k* experiment[19], performed with the Australian Earth System Model – ACCESS-ESM1.5[20]. We further assess the processes leading to the simulated subsurface warming on the Antarctic shelf.

## Results

### Subsurface warming around Antarctica

This quasi-equilibrium ACCESS-ESM1.5 *lig127k* experiment follows the CMIP6-PMIP4 experimental protocol[19] and is forced by 127 ka orbital parameters and greenhouse gases, while GrIS and AIS configurations are set at their PI levels (Methods). Compared to PI, the ACCESS-ESM1.5 *lig127k* simulation features 1.1 °C higher sea-surface temperature (SST) in the Atlantic and Indian sectors of the Southern Ocean (south of 50 °S, 70 °W–160 °E) during austral summer, as well as a ~ 1 °C higher annual mean surface air temperature over Antarctica, in agreement with most paleo-proxy records (Text S1, Fig. 4a, S2a)[21–25]. Comparison to paleo-proxy data is discussed more in-depth in Text S1.

The *lig127k* simulation displays an increase in subsurface ocean temperatures on the Antarctic shelf compared to the PI control simulation (Fig. 1a). As ice shelves can reach ~ 300 m depth and the edge of the Antarctic continental shelf lies at ~ 500 m depth, we focus our analysis on the ocean model depth 385–601 m, where the warming averages 1.3 °C in the Atlantic (70 °W–30 °E) and 1.2 °C in the Indian (30 °E–160 °E) sectors of the Southern Ocean, and extends from the Antarctic coast to 60 °S. In the Ross Sea, the warming is 0.7 °C and also extends to 60 °S, whereas the warming in the Bellinghausen and Amundsen Seas is weaker and closer to the coast. This pattern of regional temperature anomalies is maintained between 200 and 1000 m depth.

The warming extends to the sea floor south of 60 °S, with a mean temperature increase of 1.1 °C (Fig. 1d). The warming averaged across all depths is largest in the Indian sector (+1.4 °C) in particular close to the Antarctic continental slope (Fig. 2b), while ocean temperatures are 0.7 °C higher than PI in the Pacific sector (160 °E to 70 °W) (Fig. 2c). In all three basins, the warming is largest below ~1000 m depth. The oceanic temperature anomaly between LIG and PI south of 60 °S averages +1.2 °C above 1000 m (+1.5 °C below) in both the Atlantic sector and the Indian sector, and +0.3 °C (+0.9 °C below) in the Pacific sector (Fig. 2a–c).

This subsurface warming in the Southern Ocean is associated with an increase in the age of the water-masses across all depths and south of 50 °S at the LIG compared to PI (Fig. 1f). The only exception is a canyon near the Ross Sea, below 3000 m depth, which displays negative age anomalies (Fig. 1f). The simulated water-mass age is defined here as the average time since the water in a particular model grid cell has last been in contact with the surface. An 83-year increase in the mean age of the water-masses is simulated south of 60 °S, between 1000 and 3000 m depth. The largest age increase is simulated in the deep and abyssal ocean north of 50 °S, averaging +116 years below 4000 m depth. The strong relationship between changes in temperature and age suggests that the simulated increase in subsurface ocean temperatures is linked to changes in oceanic circulation (Fig. 1d, f).

### Changes in deep-ocean convection

A weakening of the lower overturning cell is simulated in our LIG experiment (Fig. 3d–f), with a 4.5 Sv weakening of Antarctic Bottom Water (AABW) transport at 30 °S compared to PI. This weakening of AABW transport is caused by a large reduction in deep-ocean convection at the LIG compared to PI in the Weddell, Lazarev and Ross Seas (Fig. 3a–c). Under PI conditions, deep ocean convection in the Weddell, Lazarev and Ross Seas brings very cold, close to freezing point, water to depth (Fig. S3a, c). Weakened deep-ocean convection at the LIG explains the relative warming and

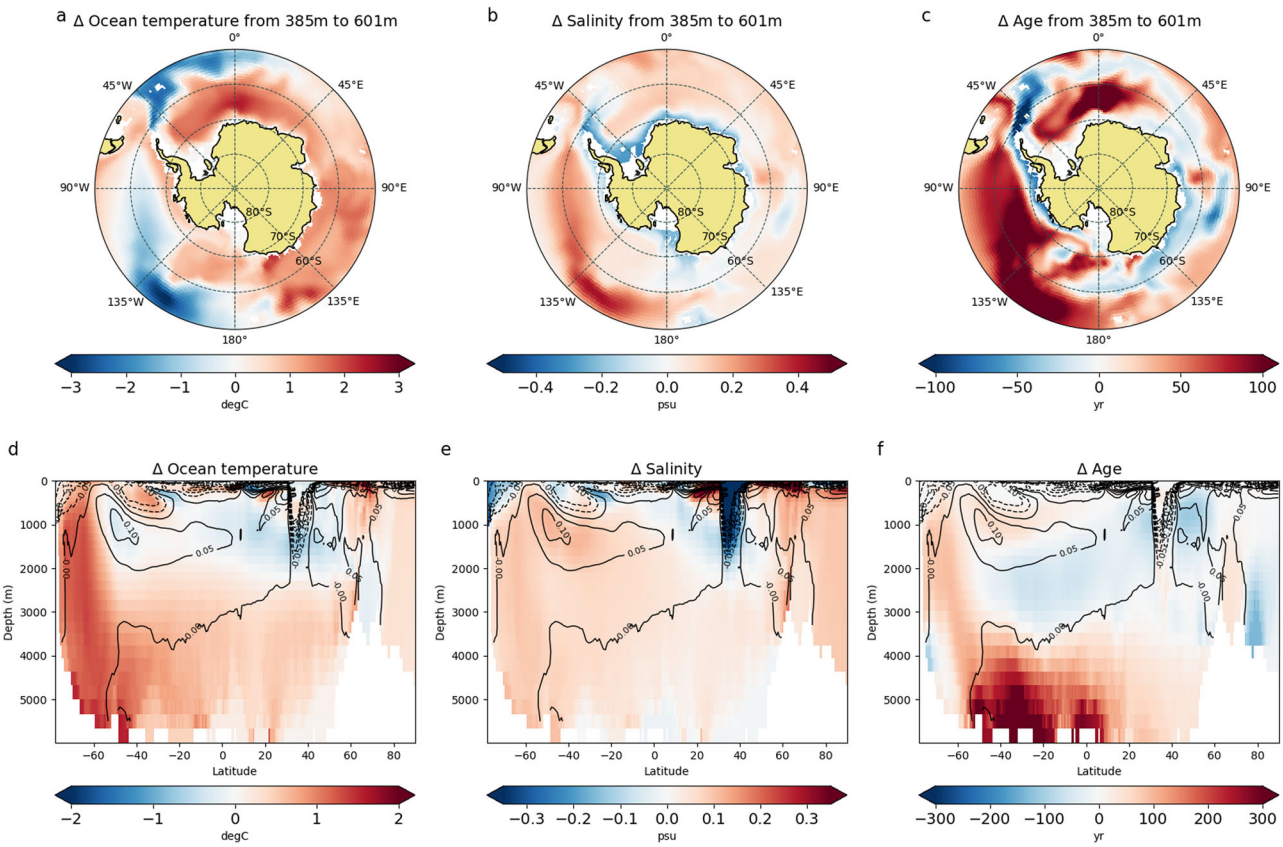


**Fig. 1 | Ocean temperature, salinity and age anomalies. a** Ocean temperature, (**b**) salinity and (**c**) age anomalies at the LIG compared to PI averaged across 385–601 m depth. Zonally-averaged (**d**) ocean temperature, (**e**) salinity, and (**f**) age anomalies (shading) with density anomalies in kg $m^{-3}$ overlaid (contours).

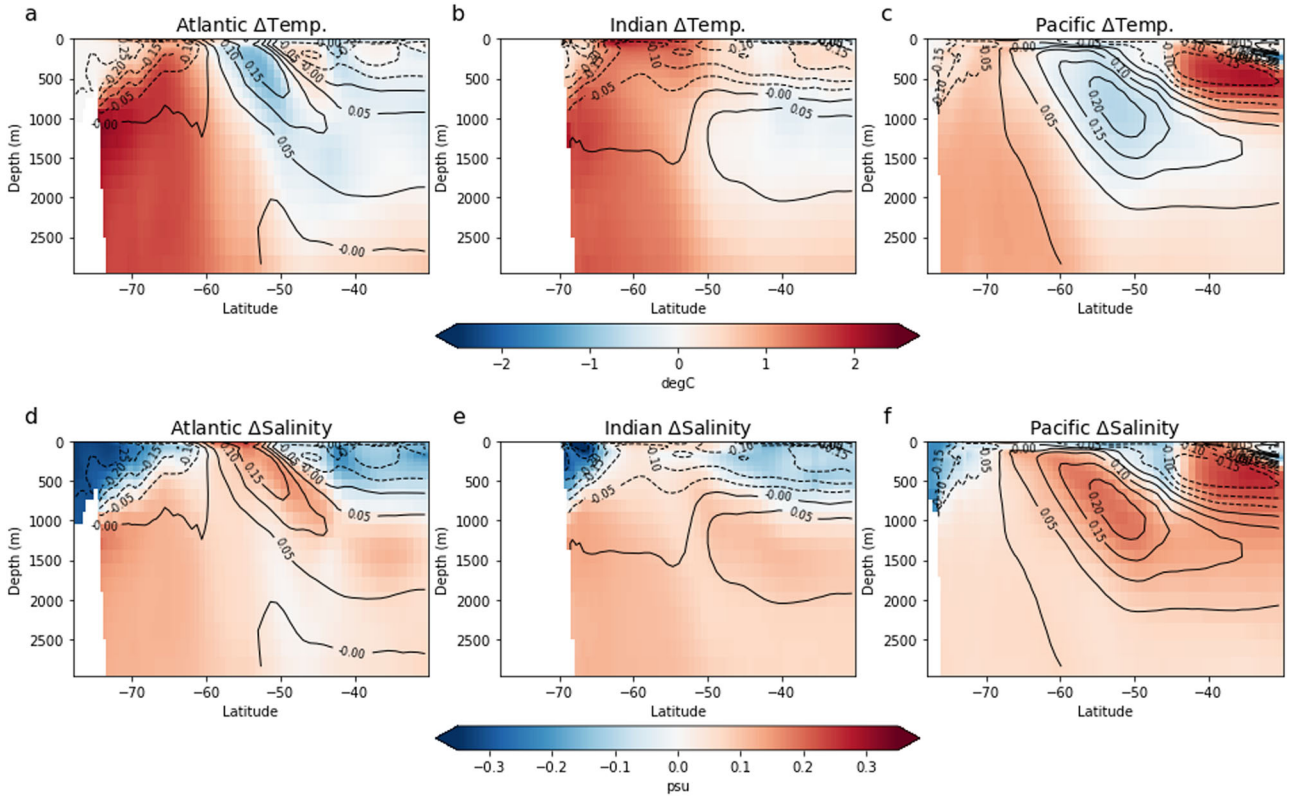


**Fig. 2 | Ocean temperature anomalies in the Atlantic, Indian and Pacific sectors of the Southern Ocean.** Zonally averaged (**a**–**c**) ocean temperature, (**d**–**f**) salinity at the LIG compared to PI over the (**a**, **d**) Atlantic (70 °W to 30 °E), (**b**, **e**) Indian (30 °E to 160 °E) and (**c**, **f**) Pacific (160 °E to 70 °W) sectors. Contours are potential density anomalies in kg $m^{-3}$.

ageing signal observed in those areas (Fig. 1a, c). The shift of convection sites (westward near the Weddell Sea and Lazarev Sea, and eastward in the Ross Sea; Fig. 3a–c) further contributes to the local warming seen in Fig. 1a. The structures of the temperature and age anomalies in the abyssal ocean are also consistent with reduced convection and weaker AABW (Fig. 1d, f).

Higher SST and lower sea-surface salinity (SSS), associated with reduced sea-ice formation on the Antarctic shelf, decrease surface water density, thus leading to reduced deep-ocean convection. The *lig127k* simulation features an annual mean SST increase of 0.7 °C south of 60 °S[25]. This is associated with an increase in poleward oceanic advective heat transport south of 50 °S in the top 200 m, reaching +0.11 PW at 55 °S (Fig. S4c, d). This contributes to a SST increase south of 60 °S of 0.4 °C in austral winter and 0.8 °C in summer compared to PI (Fig. 4a, b), and to the 41% annual-mean sea-ice area decrease (Fig. 4c, S2b, S5).

The summer sea-ice area is particularly reduced in the Weddell Sea as well as the Amundsen Sea, whereas in winter there is a large reduction in the Lazarev Sea (Fig. 4a, b). Sea-ice reduction combined with the insolation anomaly leads to an increase in downwelling shortwave radiation over the Southern Ocean throughout most of the year (Fig. S6). The total energy flux into the ocean's surface ($Q_{net}$) is higher at LIG than PI between May and October between 40 °S and 65 °S (Fig. S4a), thus leading to an annual mean positive $Q_{net}$ anomaly of 0.015 PW (Fig. S4b). $Q_{net}$ is also higher at the LIG south of 65 °S between Oct and Nov, but the annual mean anomaly is negative there (Fig. S4b).

Due to increased insolation during austral winter and spring (60 °S between days 168 and 317; Fig. S1), the annual mean sea-ice formation is reduced by 40% at the LIG compared to PI (Table 1, Fig. S7), leading to reduced brine rejection. Expectedly, there is also a 36% reduction in the annual mean sea-ice melting south of 60 °S. The net freezing south of 60 °S is 1447 Gt $yr^{-1}$ lower compared to PI, leading to fresher surface waters around Antarctica (Fig. 4d–f). The decrease in sea-ice area in turn lowers the albedo, thus enhancing the warming and further lowering the sea-ice cover. Reduced seasonality induced by the LIG orbital parameters (Fig. S1) therefore leads to reduced sea-ice formation (Table 1, Fig. S7), which lowers surface salinity in winter (Fig. 4e) and weakens the formation of deep-waters[26,27].

The annual-mean surface freshening is particularly large in the Atlantic and Indian sectors of the Southern Ocean, averaging −0.1 psu south of 65 °S (Fig. 2d,e, 4f). The negative SSS anomalies in the Indian sector (Fig. 4f) are situated closer to shore and are associated with increased sea-ice melting (Fig. S7). The freshening in the Pacific sector (-0.07 psu south of 70 °S) is relatively weaker (Fig. 2f). The freshening extends to a depth of ~1000 m but gradually decreases with depth (Fig. 1b, 2d-f). Enhanced stratification leads to positive salinity (+0.09 psu south of 60 °S) and temperature anomalies below 1000 m depth (Fig. 1e), particularly in the Atlantic and Indian sectors of the Southern Ocean (Fig. 2a, b, d, e).

In contrast, positive SSS anomalies are simulated in the seasonal sea-ice zone as well as between 60 °S and 50 °S in the Atlantic and Indian sectors (Fig. 4d-f). These positive SSS anomalies result from reduced sea-ice melting (Fig. S7) as well as stronger evaporation over precipitation (Fig. S8).

In summary, lower SSS due to a reduction of sea-ice formation, an increase in sea-ice melting in the Indian sector ( ~ 65 °S), and an increase in precipitation over Antarctica leading to higher coastal runoff (Text S2, Fig. S9), combined with warmer surface conditions, lower the density in the top ~ 1000 m at the LIG compared to PI. In contrast, the density below 2000 m depth south of 60 °S is higher at the LIG due to an increase in salinity. There is thus a strong increase in stratification in the Southern Ocean at the LIG compared to PI in our simulation.

## Advection of warm waters to East Antarctica and along the Antarctic peninsula

While the subsurface warming simulated in the Weddell, Lazarev and Ross Seas can be attributed to reduced deep-ocean convection, the subsurface

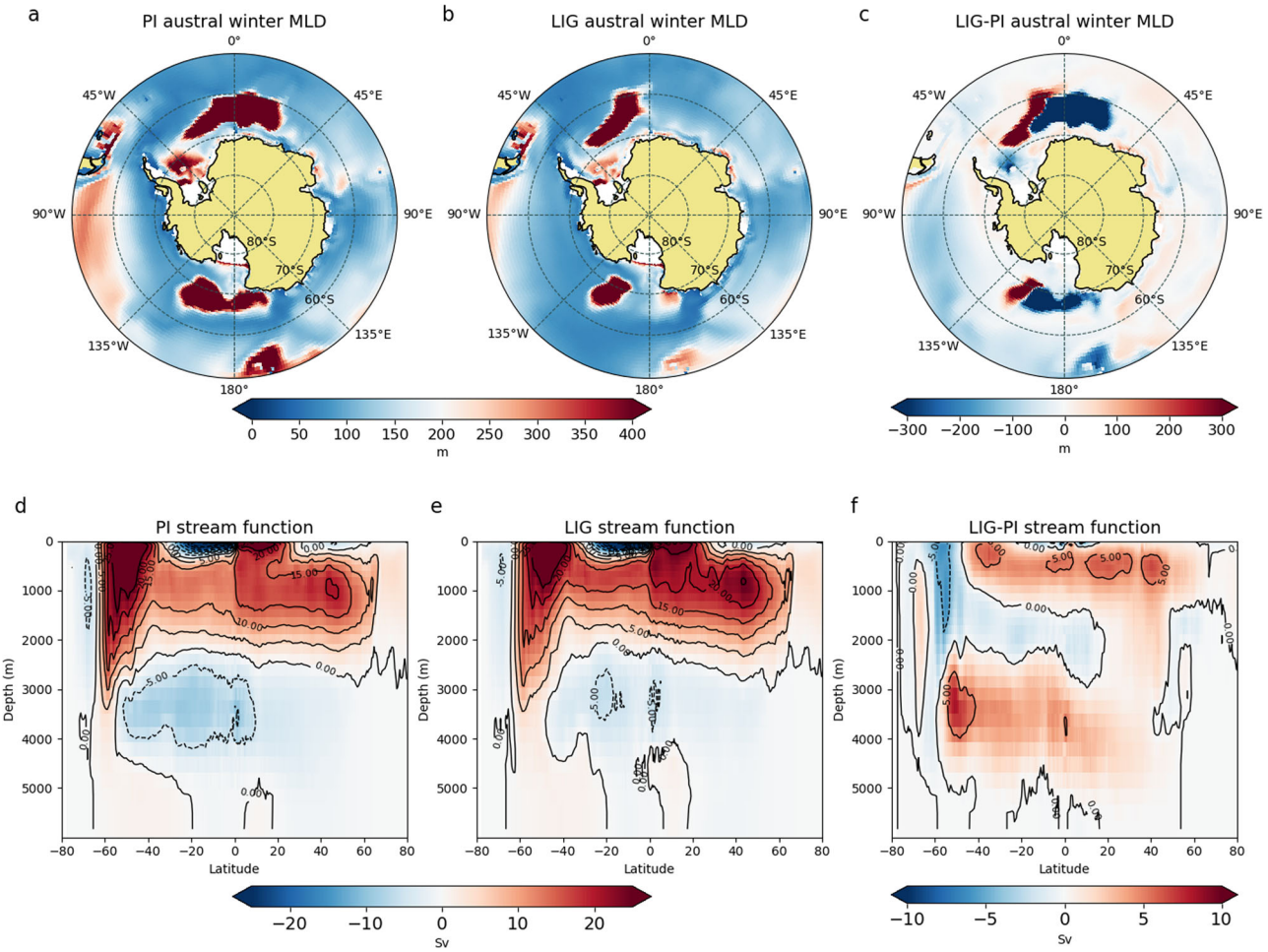


**Fig. 3 | Winter mixed layer depth (MLD) and meridional overturning stream function. a** MLD during austral winter (June to August) in PI, (**b**) LIG and (**c**) LIG-PI, and (**d**) global stream function in PI, (**e**) LIG and (**f**) LIG-PI. A paleo-calendar adjustment is applied to the LIG data in (**b**) and (**c**) such that its months have the same angular definition as PI as described in Bartlein and Shafer[68].

warming in the Indian sector of the Southern Ocean results from lateral advection of warmer waters.

Due to changes in orbital configuration, the seasonality is smaller in the southern hemisphere (Fig. S1), which affects oceanic and atmospheric circulation and heat transport at high southern latitudes. Between 60 °S and 10 °S, the meridional air temperature difference at 850 mb is 1 °C lower at the LIG than for PI (Fig. S10a). This induces a 2.5 ° equatorward shift and 7% weakening of the southern hemispheric westerlies (Fig. S10b). This wind change amplifies the temperature response as it reduces the northward Ekman transport between 50 °S and 60 °S by 19% annually and by 38% in DJF due to even weaker westerlies in austral summer (Fig. S10c). This contributes to the increase in annual mean southward oceanic heat transport south of 50 °S by up to 0.11 PW, with the strongest increase taking place between December and April (Fig. S4c,d). At the same time, polar easterly coastal winds are strengthened by 10% (Fig. 5d-f). As a result, the transition between easterly and westerly winds shifts equatorward by ~ 2 ° in most regions, except in the Pacific sector, where the boundary remains mostly unchanged.

Due to the changes in surface winds and the reduced oceanic meridional density gradient, the Antarctic Circumpolar Current weakens from 168 Sv to 116 Sv in the LIG simulation (Fig. 5c, Text S3), consistent with a recent reconstruction estimating a ~ 20% weaker ACC during the early part of the LIG and until 124 ka[28]. As the ACC acts as a barrier between the mid and high-latitude waters, the ACC weakening might contribute to the increase in southward oceanic heat transport south of 50 °S.

On the other hand, the stronger easterlies coupled with the reduction in density close to shore strengthen the Antarctic Slope Current by 28% (Fig. 5c, Text S3). As there are large horizontal pressure gradients in the frontal zone over the continental slope, thermohaline effects can intensify the wind-driven flow in the same nominal direction[29]. A freshening and warming of coastal waters in the upper 1000 m, as seen in our LIG experiment relative to PI (Fig. 2), increases the sea surface height near the coast (Fig. S11) and thus further enhances the horizontal pressure gradient, which ultimately strengthens the westward current[30].

Under PI conditions, cold waters sink in the Weddell Sea sector and contribute to deep-ocean convection. Some of these waters are advected towards the Indian sector of the Southern Ocean by the ACC (Fig. 5a, S3a, c). The combination of reduced convection northeast off the Weddell Sea, and a weakened ACC thus decreases the advection of cold waters to the Indian sector. In addition, the westward Antarctic Slope Current transports water from the Ross Sea sector towards the Indian sector. Since there is warming near the Ross Sea region at the LIG relative to PI, this warming signal is carried towards the Indian basin, contributing to the positive temperature anomalies.

Currents in the top ~ 1000 m in the Bellinghausen and Amundsen Seas are weak in our PI simulation, which is in line with observations[31] (Fig. 5a), while the ACC and thus the eastward currents across the Drake Passage are sustained. However, at the LIG the equatorward shift of the westerlies weakens the ACC and the strengthening of the easterlies induce a westward current along the Antarctic peninsula and towards the Ross Sea (Fig. 5b).

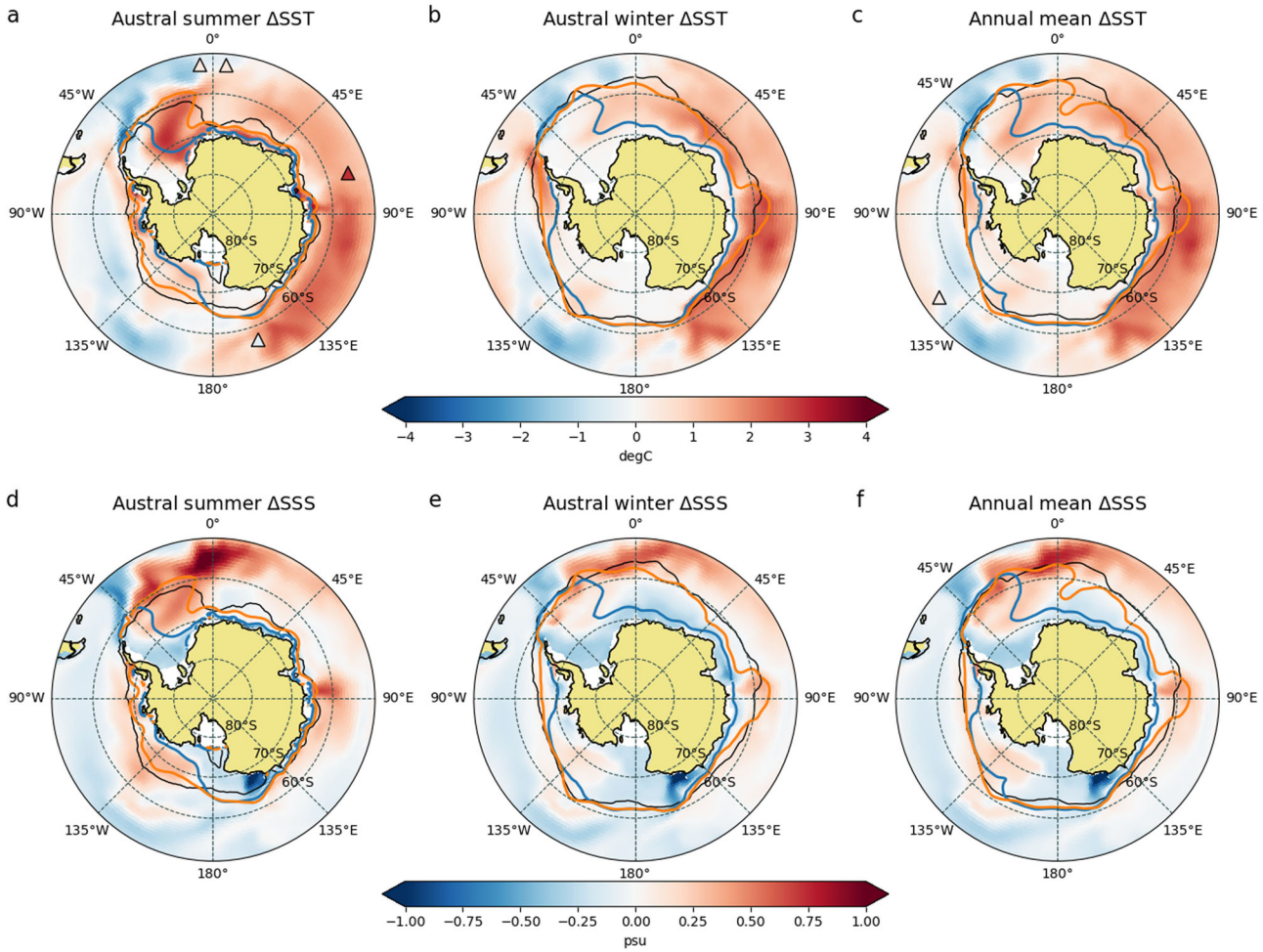


**Fig. 4 | Southern Ocean sea-surface temperature (SST) and salinity (SSS) anomalies in summer, winter, and their annual means. a** Austral summer (December to February), (**b**) austral winter (June to August), and (**c**) annual mean SST anomalies at the LIG compared to PI; and (**d**) austral summer, (**e**) austral winter, and (**f**) annual mean SSS anomalies at the LIG compared to PI, with 15% sea-ice area contours in (orange) PI, (blue) LIG, and (black) NOAA_OI_v2 dataset for 1982–2001[74] overlaid. Filled markers are proxy temperatures from the compilation by Chandler and Langebroek[23]. A paleo-calendar adjustment is applied to the LIG data in (**a**), (**b**), (**d**), and (**e**) such that its months have the same angular definition as PI as described in Bartlein and Shafer[72].

This change in ocean circulation in the Bellinghausen and Amundsen Seas brings relatively warm waters to the Antarctic shelf.

## Discussion

The AIS remains the largest potential contributor to future global sea-level rise. While the annual mean global SST at the LIG was only 0.5 °C higher than during PI[21,24], GMSL was most likely 3-6 m higher than PI, with a substantial contribution from the AIS.

Here we have shown that reduced sea-ice formation and associated higher SSTs in the Southern Ocean during the LIG reduce AABW formation and increase stratification at high southern latitudes. Reduced deep-ocean convection then leads to a subsurface warming in the Ross, Lazarev and Weddell Seas. In addition, changes in ocean currents further affect subsurface temperatures. Namely, the strengthening of the Antarctic Slope Current, which is due to a reduction in surface water density close to shore and stronger easterly winds, leads to a subsurface warming in the Indian sector of the Southern Ocean. Moreover, due to the ACC weakening, the eastward advection of cold waters from the Weddell Sea in PI is reduced at the LIG, further warming the Indian sector. Lastly, a westward current along the Antarctic peninsula and towards the Ross Sea is induced in the LIG, which transports relatively warm waters from lower latitudes to the Antarctic shelf.

**Table 1 | Freshwater flux into the ocean due to sea-ice formation and melt**

| | LIG | PI | Anom. |
|---|---|---|---|
| Melt (Gt yr$^{-1}$) | 7022 | 11043 | -4021 (-36%) |
| Freeze (Gt yr$^{-1}$) | -8341 | -13809 | 5468 (-40%) |
| Net freeze (Gt yr$^{-1}$) | -1319 | -2766 | 1447 (-52%) |

Total annual freshwater flux between sea-ice and ocean south of 60 °S (positive values indicate freshwater addition to the ocean).

It should however be noted that instead of being formed by dense water export from the Antarctic continental shelf, AABW is formed via deep ocean convection in the ACCESS-ESM1.5, as is the case for 77% of the CMIP6 models[32]. In addition, as is the case for most if not all CMIP6 models, the ACCESS-ESM1.5 relies on the Gent-McWilliams (GM) parameterisation to represent the transport associated with mesoscale eddies[33]. Despite this, the ACCESS-ESM1.5 provides a reasonable representation of the state of the Southern Ocean which includes a reasonable representation of the temperature and density of the Antarctic Shelf Bottom Water[34] and of the Southern Ocean sea-ice cover[20]. While it would be preferable to repeat a similar study with an eddy-rich model, no such simulations currently exist for the LIG.

The simulated ACCESS-ESM1.5 PI Antarctic sea-ice area is in agreement with observations in austral summer, while the simulated austral winter sea-ice area is slightly underestimated. The simulated LIG sea-ice area is well within the spread of other CMIP6-PMIP4 models[35].

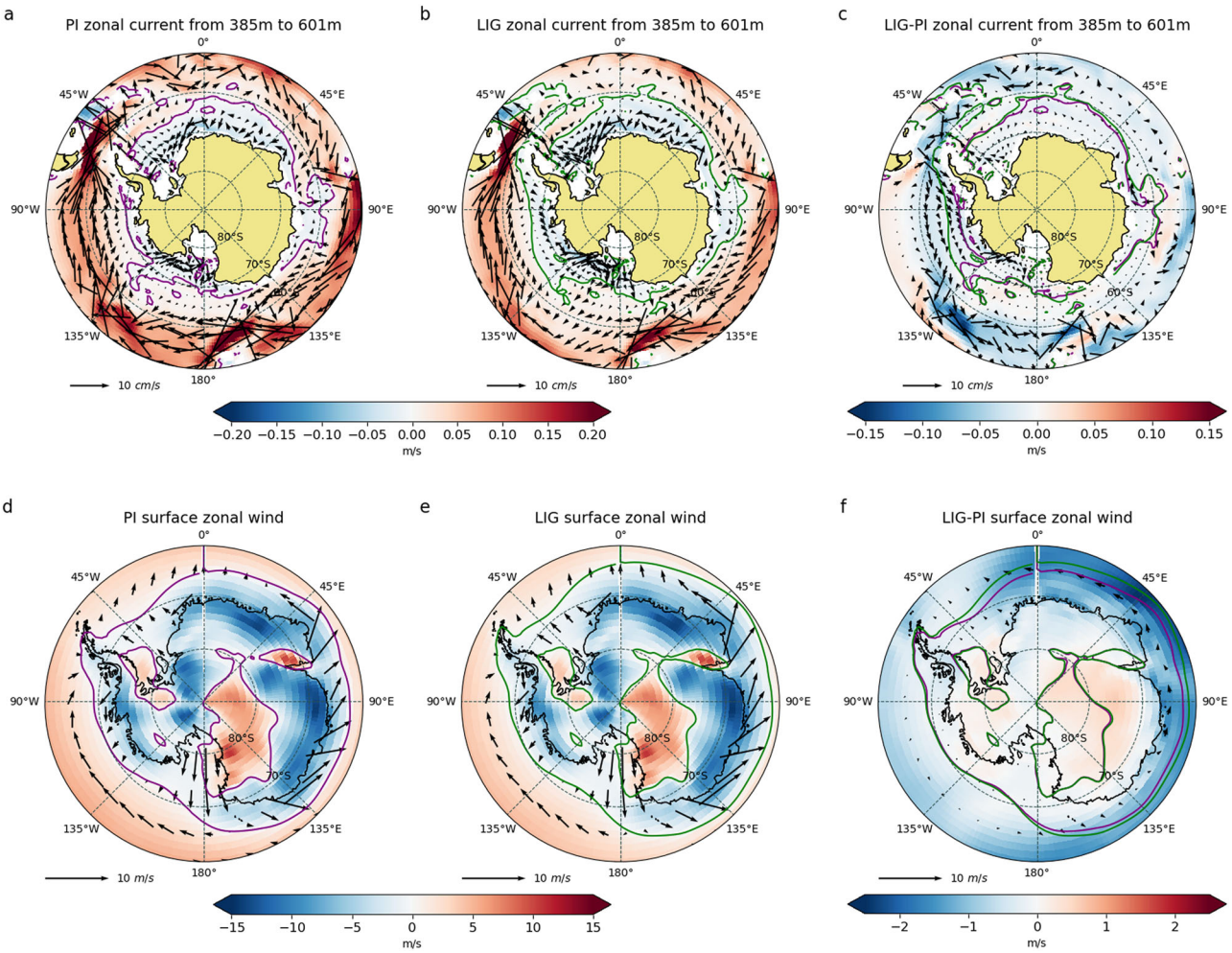


**Fig. 5 | Subsurface ocean zonal currents and surface zonal winds over the Southern Ocean.** Ocean zonal currents averaged across 385-601 m depth at (**a**) PI, (**b**) LIG and (**c**) LIG-PI, and surface zonal winds at (**d**) PI, (**e**) LIG and (**f**) LIG-PI. Colour shading represents the intensity of the zonal velocity components, while the overlain arrows are the full current/wind vectors which include the meridional components. Contour lines mark the boundaries at which the zonal component are zero at (purple) PI and (green) LIG.

While the simulated Antarctic sea-ice anomalies in the ACCESS-ESM1.5 are the largest of the CMIP6-PMIP4 models, with a ~ 50% smaller LIG winter Antarctic sea-ice area compared to present-day observations (Fig. S5), it is in agreement with a previous study[36], which suggested that a 65% reduction in winter Antarctic sea-ice area was consistent with the ice core evidence at 128 ka. This reduced sea-ice cover is associated with higher high-latitude surface air temperatures (Fig. S2a). Lower sea-ice concentration leads to warmer air above as the albedo decreases, which explains the relatively strong warming of surface air between 60 °S and 80 °S in the *lig127k* ACCESS-ESM1.5 experiment. While this high latitude surface air temperature anomaly is ~ 2 °C higher than the CMIP6-PMIP4 multi-model mean, it is in agreement with the other models that simulate lower Antarctic sea-ice cover at the LIG[35], and this warming is still lower than the one estimated from ice-core records (Text S1)[35]. In agreement with more than 70% of the PMIP4 *lig127k* simulations, the maximum surface warming is simulated to the east of the Weddell Sea, extending into the Indian sector of the Southern Ocean[35]. This warming could be due to a decrease in winter sea-ice in most models. This region might be particularly sensitive to warming as it corresponds to the northernmost position of the sea-ice edge today[37].

As the annual mean insolation at high latitudes increases with obliquity[38], numerical simulations have shown that higher obliquity weakens the meridional SST gradient in the Southern Ocean[39,40] and leads to a lower sea-ice cover. With obliquity at *lig127k* being higher than today (24.04° vs 23.46°), our simulated warming in the Southern Ocean and reduced sea-ice cover are in line with these findings. Furthermore, our simulated equatorward shift and weakening of the southern hemispheric westerlies under low precession at the LIG is consistent with the study of Persch et al.[41], who found that high precession leads to a strengthening and poleward shift of the westerlies.

While our *lig127k* simulation displays freshening and increased stratification in the Southern Ocean mainly due to increased sea-ice melting, potential freshwater flux from ice shelf and iceberg melt or enhanced basal melt from Antarctica are not included here. Previous studies have shown that enhanced freshwater flux in the Southern Ocean, such as one that would result from a partial disintegration of the AIS, would cool the surface ocean by 1 to 2 °C[42–44] and lead to a sea-ice advance[45,46], thus reducing the Southern Ocean surface warming. However, the meltwater input would also enhance stratification and reduce AABW formation, thus increasing the subsurface warming[42,44,47].

AIS modelling studies have suggested that a ~ 3 °C subsurface warming compared to PI on the Antarctic shelf is required to trigger a partial collapse of the WAIS and of some basins of the EAIS during warm interglacials[16–18]. However, some ice sheet modeling work has shown that a sustained retreat of the WAIS can occur over the coming centuries even with present-day melt rates[48,49]. Our LIG simulation exhibits a subsurface warming on the Antarctic shelf, averaging +0.8 °C at 385-601 m depth south of 60 °S. Across the same depths, the Atlantic sector has the highest warming (+1.3 °C mean,

+2.4 °C maximum), followed by the Indian sector (+1.2 °C mean, +2.2 °C maximum), indicating that the LIG subsurface warming on the Antarctic shelf could have triggered substantial ice-mass loss from the AIS. AABW formation is responsible for drawing cold, salty, dense waters into the deep and abyssal ocean during winter sea-ice formation, and is sensitive to changes in upper ocean density[50,51]. Weaker AABW formation can thus lead to a subsurface warming around Antarctica, potentially giving rise to increased ice-flux from the AIS, which would further weaken AABW formation, thus creating a positive feedback[42,52,53].

Such a subsurface warming is simulated under full LIG conditions, and is associated with a weaker AABW but stronger North Atlantic Deep Water formation compared to PI. This complements previous studies, which have suggested that the rapid AIS disintegration during the penultimate deglaciation and early part of the LIG was a result of the long Atlantic Meridional Overturning Circulation shutdown that occurred during Heinrich stadial 11[54,55]. While these studies suggest that a loss of AIS mass beyond its PI level could have been the result of the transient deglacial climate response, here we show that increased ice-flux from the AIS could also result from increases in surface air, sea surface and subsurface temperature that arise from equilibrium interglacial conditions. This is consistent with Southern Ocean sediment records suggesting decreased oxygenation of deep waters at 127 ka, implying a reduction of AABW formation during peak LIG conditions[14]. There is also evidence of ice-mass loss from the Wilkes Subglacial Basin during the maximum high southern latitudes warmth at the onset of the LIG, though it might not have manifested from LIG equilibrium conditions due to its early timing[16].

While future warming is primarily driven by increased $CO_2$, the climatic differences between PI and LIG as simulated here are due to variations in orbital configuration. The reduction of Antarctic sea-ice and increased heat transport into the Southern Ocean simulated in this study might be specific to the radiative forcing at the LIG, but this serves as an example that considerable subsurface warming on the Antarctic shelf can be achieved by a decline in sea-ice and the associated reduction in deep-ocean convection.

A subsurface ocean warming has contributed to the melting and thinning of West Antarctic ice shelves in recent decades[56,57]. While Southern Ocean sea-ice extent has increased slowly at the end of the 20th century and until 2016, it has abruptly decreased since then[58], hinting at an accelerated warming of the Southern Ocean. In addition, modern observations indicate the surface Southern Ocean has freshened since the 1950s due to increased melting of AIS, thus weakening deep ocean convection and AABW formation[50]. AABW has warmed over recent decades, leading to higher temperatures in the deep Southern Ocean and global abyssal waters[59,60]. A Southern Ocean sea-ice decline over the coming century could further increase ocean stratification around Antarctica, thus accelerating AIS mass loss and global sea-level rise.

## Methods

The results presented in this study are from the Australian Community Climate and Earth System Simulator (ACCESS-ESM1.5)[20], which is a fully coupled atmosphere-land-ocean-sea-ice-carbon-cycle model.

The ACCESS-ESM1.5 includes the UK Met Office Unified Model version 7.3 (UM7.3)[61,62] as its atmospheric component with a resolution of 1.875° longitude by 1.25° latitude and 38 vertical levels. The land surface model, Community Atmosphere Biosphere Land Exchange model (CABLE2.4)[63], is coupled to UM7.3. It is configured with 13 plant functional types (10 vegetated and 3 non-vegetated types), and their spatial distribution is fixed such that the vegetation is static, but the leaf area index is interactive in the model.

The ocean component of the ACCESS-ESM1.5 is the NOAA/GFDL Modular Ocean Model version 5 (MOM5)[64], which has a nominal resolution of 1° with 50 vertical grid levels, and has higher resolution near the equator (0.33°) and in the Southern Ocean ( ~ 0.4° at 70 °S). It relies on a flow-dependent GM parameterisation[33] to represent the transport associated with mesoscale eddies as described in Kiss et al.[65]. The ocean configuration is similar to the ACCESS1.0 and ACCESS1.3[66]. The LANL CICE4.1 model[67] simulates sea-ice with five thickness classes, and has the same horizontal grid as the ocean model. Ocean biogeochemistry is simulated by the Whole Ocean Model of Biogeochemistry And Trophic-dynamics (WOMBAT)[68,69]. The OASIS-MCT[70] couples the ocean and sea ice to the atmosphere. A brief description of the model's performances under present-day conditions is included in Text S1.

The initial conditions of the *lig127k* experiment are based on a PI simulation (1850 CE; *piControl*)[20], which follows the CMIP6 protocol[71]. Orbital parameters are set at the year 1850 and the greenhouse gas concentrations are the following: $CO_2$ at 284.3 ppm, $CH_4$ at 808.2 ppb, and $N_2O$ at 273.0 ppb. The *piControl* run also serves as a reference in this study.

The *lig127k* experiment follows the CMIP6-PMIP4 protocol with appropriate 127 ka orbital parameters and greenhouse gas concentrations (i.e., $CO_2$ at 275 ppm, $CH_4$ at 685 ppb and $N_2O$ at 255 ppb)[19,25]. Continental ice sheets and vegetation cover are constant and are the same as prescribed in *piControl*. The *lig127k* experiment was integrated for 650 years, and 1000 years for *piControl*. Results from their last 100 years are used here. The quasi-equilibrium state and drifts of *lig127k* are discussed in Text S4. A paleo-calendar adjustment was performed on all the seasonal data presented in this study (Figs. 3b, c, 4, S5, and S10b-c) using the program described in Bartlein and Shafer[72], except for data associated with energy flux (Fig. S1, S4, and S6).

## Data availability

All data needed to evaluate the conclusions in the paper are present in the paper and/or the Supplementary Materials. The model results of the *lig127k* simulation are archived on the CMIP6 ESGF website[73].

Received: 11 July 2023; Accepted: 10 April 2024;
Published online: 20 April 2024

## References

1. Past Interglacials Working Group Of PAGES. Interglacials of the last 800,000 years. *Rev. Geophys.* **54**, 162–219 (2016).
2. Meinshausen, M. et al. Historical greenhouse gas concentrations for climate modelling (cmip6). *Geosci. Model Dev.* **10**, 2057–2116 (2017).
3. Dutton, A. & Lambeck, K. Ice volume and sea level during the last interglacial. *Science* **337**, 216–219 (2012).
4. Dyer, B. et al. Sea-level trends across the bahamas constrain peak last interglacial ice melt. *Proc. Nat. Acad. Sci.* **118**, e2026839118 (2021).
5. Kopp, R. E., Simons, F. J., Mitrovica, J. X., Maloof, A. C. & Oppenheimer, M. Probabilistic assessment of sea level during the last interglacial stage. *Nature* **462**, 863–867 (2009).
6. Capron, E. et al. Challenges and research priorities to understand interactions between climate, ice sheets and global mean sea level during past interglacials. *Quaternary Sci. Rev.* **219**, 308–311 (2019).
7. Rohling, E. J. et al. Asynchronous antarctic and greenland ice-volume contributions to the last interglacial sea-level highstand. *Nat. Commun.* **10**, 5040 (2019).
8. Shackleton, S. et al. Global ocean heat content in the last interglacial. *Nat. Geosci.* **13**, 77–81 (2020).
9. Colville, E. J. et al. Sr-nd-pb isotope evidence for ice-sheet presence on southern greenland during the last interglacial. *Science* **333**, 620–623 (2011).
10. Dutton, A. et al. Sea-level rise due to polar ice-sheet mass loss during past warm periods. *Science* **349**, aaa4019 (2015).
11. NEEM community members. Eemian interglacial reconstructed from a greenland folded ice core. *Nature* **493**, 489–494 (2013).
12. Yau, A. M., Bender, M. L., Robinson, A. & Brook, E. J. Reconstructing the last interglacial at summit, greenland: Insights from gisp2. *Proc. Nat. Acad. Sci.* **113**, 9710 (2016).
13. Barnett, R. L. et al. Constraining the contribution of the antarctic ice sheet to last interglacial sea level. *Sci. Adv.* **9**, eadf0198 (2023).
14. Hayes, C. T. et al. A stagnation event in the deep south atlantic during the last interglacial period. *Science* **346**, 1514–1517 (2014).

15. Turney, C. S. M. et al. Early last interglacial ocean warming drove substantial ice mass loss from antarctica. *Proc. Nat. Acad. Sci.* **117**, 3996–4006 (2020).
16. Wilson, D. J. et al. Ice loss from the east antarctic ice sheet during late pleistocene interglacials. *Nature* **561**, 383–386 (2018).
17. DeConto, R. M. & Pollard, D. Contribution of antarctica to past and future sea-level rise. *Nature* **531**, 591 EP – (2016).
18. Tigchelaar, M., Timmermann, A., Pollard, D., Friedrich, T. & Heinemann, M. Local insolation changes enhance antarctic interglacials: Insights from an 800,000-year ice sheet simulation with transient climate forcing. *Earth Planetary Sci. Lett.* **495**, 69–78 (2018).
19. Otto-Bliesner, B. L. et al. The pmip4 contribution to cmip6 – part 2: Two interglacials, scientific objective and experimental design for holocene and last interglacial simulations. *Geosci. Model Dev.* **10**, 3979–4003 (2017).
20. Ziehn, T. et al. The australian earth system model: Access-esm1.5. *J. Southern Hemisphere Earth Syst. Sci.* **70**, 193–214 (2020).
21. Capron, E. et al. Temporal and spatial structure of multi-millennial temperature changes at high latitudes during the last interglacial. *Quaternary Sci. Rev.* **103**, 116–133 (2014).
22. Capron, E., Govin, A., Feng, R., Otto-Bliesner, B. & Wolff, E. Critical evaluation of climate syntheses to benchmark cmip6/pmip4 127 ka last interglacial simulations in the high-latitude regions. *Quaternary Sci. Rev.* **168**, 137–150 (2017).
23. Chandler, D. & Langebroek, P. Southern ocean sea surface temperature synthesis: Part 2. penultimate glacial and last interglacial. *Quaternary Sci. Rev.* **271**, 107190 (2021).
24. Hoffman, J. S., Clark, P. U., Parnell, A. C. & He, F. Regional and global sea-surface temperatures during the last interglaciation. *Science* **355**, 276–279 (2017).
25. Yeung, N. et al. Land–sea temperature contrasts at the last interglacial and their impact on the hydrological cycle. *Clim. Past* **17**, 869–885 (2021).
26. Gill, A. Circulation and bottom water production in the weddell sea. *Deep Sea Res. Oceanogr. Abstr.* **20**, 111–140 (1973).
27. Ohshima, K. I. et al. Antarctic bottom water production by intense sea-ice formation in the cape darnley polynya. *Nat. Geosci.* **6**, 235–240 (2013).
28. Wu, S. et al. Orbital- and millennial-scale antarctic circumpolar current variability in drake passage over the past 140,000 years. *Nat. Commun.* **12**, 3948 (2021).
29. Fahrbach, E., Rohardt, G. & Krause, G. The antarctic coastal current in the southeastern weddell sea. *Polar Biol.* **12**, 171–182 (1992).
30. Fahrbach, E., Peterson, R., Rohardt, G., Schlosser, P. & Bayer, R. Suppression of bottom water formation in the southeastern weddell sea. *Deep Sea Res. Part I: Oceanogr. Res. Papers* **41**, 389–411 (1994).
31. Thompson, A. F., Stewart, A. L., Spence, P. & Heywood, K. J. The antarctic slope current in a changing climate. *Rev. Geophys.* **56**, 741–770 (2018).
32. Heuzé, C. Antarctic bottom water and north atlantic deep water in cmip6 models. *Ocean Sci.* **17**, 59–90 (2021).
33. Gent, P. R. & Mcwilliams, J. C. Isopycnal mixing in ocean circulation models. *J. Phys. Oceanogr.* **20**, 150 – 155 (1990).
34. Purich, A. & England, M. H. Historical and future projected warming of antarctic shelf bottom water in cmip6 models. *Geophys. Res. Lett.* **48**, e2021GL092752 (2021).
35. Otto-Bliesner, B. L. et al. Large-scale features of last interglacial climate: results from evaluating the *lig127k* simulations for the coupled model intercomparison project (cmip6)–paleoclimate modeling intercomparison project (pmip4). *Clim. Past* **17**, 63–94 (2021).
36. Holloway, M. D. et al. Antarctic last interglacial isotope peak in response to sea ice retreat not ice-sheet collapse. *Nature Commun.* **7**, 12293 (2016).
37. Rayner, N. A. et al. Global analyses of sea surface temperature, sea ice, and night marine air temperature since the late nineteenth century. *J. Geophys. Res.: Atmosph.* **108**, 4407 (2003).
38. Loutre, M.-F., Paillard, D., Vimeux, F. & Cortijo, E. Does mean annual insolation have the potential to change the climate? *Earth Planetary Sci. Lett.* **221**, 1–14 (2004).
39. Timmermann, A. et al. Modeling obliquity and co2 effects on southern hemisphere climate during the past 408 ka. *J. Clim.* **27**, 1863 – 1875 (2014).
40. Wu, Z., Yin, Q., Guo, Z. & Berger, A. Hemisphere differences in response of sea surface temperature and sea ice to precession and obliquity. *Global Planet. Change* **192**, 103223 (2020).
41. Persch, C. F., DiNezio, P. & Lovenduski, N. S. The impact of orbital precession on air-sea co2 exchange in the southern ocean. *Geophys. Res. Lett.* **50**, e2023GL103820 (2023).
42. Menviel, L., Timmermann, A., Timm, O. E. & Mouchet, A. Climate and biogeochemical response to a rapid melting of the west antarctic ice sheet during interglacials and implications for future climate. *Paleoceanography* **25**, PA4231 (2010).
43. Fogwill, C. J., Phipps, S. J., Turney, C. S. M. & Golledge, N. R. Sensitivity of the southern ocean to enhanced regional antarctic ice sheet meltwater input. *Earth's Future* **3**, 317–329 (2015).
44. Hutchinson, D. K., Menviel, L., Meissner, K. J. & Hogg, A. M. East antarctic warming forced by ice loss during the last interglacial. *Nat. Commun.* **15**, 1026 (2024).
45. Bintanja, R., van Oldenborgh, G. J., Drijfhout, S. S., Wouters, B. & Katsman, C. A. Important role for ocean warming and increased ice-shelf melt in antarctic sea-ice expansion. *Nat. Geosci.* **6**, 376–379 (2013).
46. Pauling, A. G., Bitz, C. M., Smith, I. J. & Langhorne, P. J. The response of the southern ocean and antarctic sea ice to freshwater from ice shelves in an earth system model. *J. Clim.* **29**, 1655 – 1672 (2016).
47. Bronselaer, B. et al. Change in future climate due to antarctic meltwater. *Nature* **564**, 53–58 (2018).
48. Arthern, R. J. & Williams, C. R. The sensitivity of west antarctica to the submarine melting feedback. *Geophys. Res. Lett.* **44**, 2352–2359 (2017).
49. Golledge, N. R. et al. Retreat of the antarctic ice sheet during the last interglaciation and implications for future change. *Geophys. Res. Lett.* **48**, e2021GL094513 (2021).
50. de Lavergne, C., Palter, J. B., Galbraith, E. D., Bernardello, R. & Marinov, I. Cessation of deep convection in the open southern ocean under anthropogenic climate change. *Nat. Clim. Change* **4**, 278–282 (2014).
51. Snow, K., Hogg, A. M., Sloyan, B. M. & Downes, S. M. Sensitivity of antarctic bottom water to changes in surface buoyancy fluxes. *J. Clim.* **29**, 313 – 330 (2016).
52. Golledge, N. R. et al. Antarctic contribution to meltwater pulse 1a from reduced southern ocean overturning. *Nat. Commun.* **5**, 5107 (2014).
53. Weber, M. E. et al. Millennial-scale variability in antarctic ice-sheet discharge during the last deglaciation. *Nature* **510**, 134–138 (2014).
54. Clark, P. U. et al. Oceanic forcing of penultimate deglacial and last interglacial sea-level rise. *Nature* **577**, 660–664 (2020).
55. Marino, G. et al. Bipolar seesaw control on last interglacial sea level. *Nature* **522**, 197 EP – (2015).
56. Benn, D. I. et al. Rapid fragmentation of thwaites eastern ice shelf, west antarctica. *Cryosph. Disc.* **2021**, 1–25 (2021).
57. Paolo, F. S., Fricker, H. A. & Padman, L. Volume loss from antarctic ice shelves is accelerating. *Science* **348**, 327–331 (2015).
58. Eayrs, C., Li, X., Raphael, M. N. & Holland, D. M. Rapid decline in antarctic sea ice in recent years hints at future change. *Nat. Geosci.* **14**, 460–464 (2021).
59. Johnson, G. C., McTaggart, K. E. & Wanninkhof, R. Antarctic bottom water temperature changes in the western south atlantic from 1989 to 2014. *J. Geophys. Res.: Oceans* **119**, 8567–8577 (2014).
60. Purkey, S. G. & Johnson, G. C. Warming of global abyssal and deep southern ocean waters between the 1990s and 2000s:

Contributions to global heat and sea level rise budgets. *J. Climate* **23**, 6336–6351 (2010).
61. The HadGEM2 Development Team. The hadgem2 family of met office unified model climate configurations. *Geosci. Model Dev.* **4**, 723–757 (2011).
62. Martin, G. M. et al. Analysis and reduction of systematic errors through a seamless approach to modeling weather and climate. *J. Clim.* **23**, 5933–5957 (2010).
63. Kowalczyk, E. et al. The land surface model component of ACCESS: description and impact on the simulated surface climatology. *Australian Meteorological and Oceanographic Journal* **63**, 65–82 (2013).
64. Griffies, S. M. Elements of the Modular Ocean Model (MOM): 2012 release. GFDL Ocean Group Tech. Rep. 7. NOAA/Geophysical Fluid Dynamics Laboratory, Princeton, NJ, 618 pp. (2012).
65. Kiss, A. E. et al. Access-om2 v1.0: a global ocean–sea ice model at three resolutions. *Geosci. Model Dev.* **13**, 401–442 (2020).
66. Bi, D. et al. The access coupled model: Description, control climate and evaluation. *Austr. Meteorolog. Oceanogr. J.* **63**, 41–64 (2012).
67. Hunke, E. C. & Lipscomb, W. H. Cice: The los alamos sea ice model. documentation and software user's manual version 4.1, tech. rep. la cc 06 012. Tech. Rep., T 3 Fluid Dyn. Group, Los Alamos Natl. Lab., Los Alamos, N. M. (2010).
68. Law, R. M. et al. The carbon cycle in the Australian Community Climate and Earth System Simulator (ACCESS-ESM1) – Part 1: Model description and pre-industrial simulation. *Geosci. Model Dev.* **10**, 2567–2590 (2017).
69. Oke, P. R. et al. Evaluation of a near-global eddy-resolving ocean model. *Geosci Model Dev.* **6,** 591–615 (2013).
70. Valcke, S. The oasis3 coupler: a european climate modelling community software. *Geosci. Model Dev.* **6**, 373–388 (2013).
71. Eyring, V. et al. Overview of the coupled model intercomparison project phase 6 (cmip6) experimental design and organization. *Geosci. Model Dev.* **9**, 1937–1958 (2016).
72. Bartlein, P. J. & Shafer, S. L. Paleo calendar-effect adjustments in time-slice and transient climate-model simulations (paleocaladjust v1.0): impact and strategies for data analysis. *Geosci. Model Dev* **12**, 3889–3913 (2019).
73. Yeung, N. et al. CSIRO ACCESS-ESM1.5 model output prepared for CMIP6 PMIP lig127k. *Earth System Grid Federation* https://doi.org/10.22033/ESGF/CMIP6.13703 (2019).
74. Reynolds, R. W., Rayner, N. A., Smith, T. M., Stokes, D. C. & Wang, W. An improved in situ and satellite sst analysis for climate. *J. Climate* **15**, 1609 – 1625 (2002).

## Acknowledgements

Computational resources were provided by the NCI National Facility at the Australian National University, through awards under the Merit Allocation Scheme and the UNSW HPC at NCI scheme. KJM and LM acknowledge support from the Australian Research Council (DP180100048, FT180100606 and SR200100008). NKHY acknowledges the Research Training Program provided by the Australian government, a top-up scholarship provided by the Climate Change Research Centre, and support from the ARC Centre of Excellence for Climate Extremes.

## Author contributions

LM and KJM designed the study. NY performed the LIG numerical experiment. TZ and MC contributed to the model setup, performed the PI experiment and helped with the post-processing of the numerical outputs. NY performed the data analysis with the help of DC and under the guidance of LM and KJM. NY and LM wrote the manuscript with contributions from all authors.

## Competing interests

The authors declare no competing interests.

## Additional information

**Supplementary information** The online version contains supplementary material available at https://doi.org/10.1038/s43247-024-01383-x.

**Correspondence** and requests for materials should be addressed to Nicholas King-Hei Yeung.

**Peer review information** *Communications Earth & Environment* thanks Pepijn Bakker and the other, anonymous, reviewer(s) for their contribution to the peer review of this work. Primary Handling Editors: Helen McGregor, Alireza Bahadori and Aliénor Lavergne. A peer review file is available.